JOURNAL OF GUIDANCE, CONTROL, AND DYNAMICS
Vol. 34, No. 1, January–February 2011

Identification of Multimodal Pilot Models Using Ramp Target and Multisine Disturbance Signals

D. M. Pool,* P. M. T. Zaal,† M. M. van Paassen,‡ and M. Mulder§
Delft University of Technology, 2600 GB Delft, The Netherlands

DOI: 10.2514/1.50612

This paper investigates the extent to which target forcing functions consisting of multiple ramplike or steplike changes in target attitude can be used for identification of multimodal pilot models. The main question addressed is whether such signals provide enough excitation of the pilot–vehicle system to allow for reliable estimation of pilot model parameters from measured pilot control data. The compensatory control task from a previous human-in-the-loop experiment performed in a moving base flight simulator is used to define a typical multimodal pilot model identification problem. Using simulations of this control task, where different multisine and ramp target forcing function signals are used to excite the pilot–vehicle system (in addition to a multisine disturbance signal), the accuracy and consistency of pilot model estimation results are evaluated. It is found that both the bias and variance of the pilot model parameter estimates decrease with increasing ramp signal steepness. If the steepnesses of the ramps in the target signals are higher than 3 deg/s, estimation results are found to be more accurate than those obtained using a quasi-random target forcing function. This indicates that reliable pilot model identification results can be obtained using such ramp target forcing function signals.

Nomenclature

A	=	ramp and step final magnitudes
$A(k)$	=	amplitude of k^{th} sinusoid, deg
D	=	Lilliefors test statistic
e	=	tracking error signal, rad
$F(j\omega)$	=	forcing function Fourier transform
f	=	probability density function
f_d	=	disturbance forcing function, rad
f_t	=	target forcing function, rad
$H(j\omega)$	=	frequency response function
$H(s)$	=	transfer function
H_c	=	controlled element dynamics
H_n	=	remnant filter
H_{nm}	=	neuromuscular system dynamics
H_{p_v}	=	pilot visual response
H_{p_m}	=	pilot motion response
H_{scc}	=	semicircular canal dynamics
j	=	imaginary unit
K_c	=	controlled element gain
K_n	=	remnant filter gain
K_{p_m}	=	pilot motion gain
K_{p_v}	=	pilot visual gain
K_{scc}	=	semicircular canal dynamics gain
$K_{\delta,u}$	=	stick output gain
k	=	sinusoid index
N	=	number of sinusoids
n	=	remnant signal, rad
$n(k)$	=	frequency integer factor for k^{th} sinusoid
p	=	Lilliefors test significance value
$R(s)$	=	ramp signal Laplace transform
$r(t)$	=	ramp signal
$S(s)$	=	step signal Laplace transform
s	=	Laplace operator
$s(t)$	=	step signal
T	=	ramp signal rise time, s
T_L	=	pilot visual lead time constant, s
T_n	=	remnant filter time constant, s
t	=	time, s
u	=	manipulator deflection, rad
x	=	controlled element state, rad
δ	=	controlled element input, rad
ζ_{nm}	=	neuromuscular damping
μ	=	mean
σ	=	standard deviation
σ^2	=	variance
$\phi(k)$	=	phase shift of k^{th} sinusoid, rad
τ_m	=	pilot motion time delay, s
τ_v	=	pilot visual time delay, s
ω	=	frequency, rad $\cdot$ s^{-1}
$\omega(k)$	=	frequency of k^{th} sinusoid, rad $\cdot$ s^{-1}
ω_{nm}	=	neuromuscular frequency, rad $\cdot$ s^{-1}

Subscripts

d	=	disturbance forcing function
t	=	target forcing function

Received 4 May 2010; revision received 8 June 2010; accepted for publication 14 June 2010.

*Ph.D. Candidate, Control and Simulation Division, Faculty of Aerospace Engineering, P.O. Box 5058; d.m.pool@tudelft.nl. Student Member AIAA.

†Ph.D. Candidate, Control and Simulation Division, Faculty of Aerospace Engineering, P.O. Box 5058; p.m.t.zaal@tudelft.nl. Student Member AIAA.

‡Associate Professor, Control and Simulation Division, Faculty of Aerospace Engineering, P.O. Box 5058; m.m.vanpaassen@tudelft.nl. Member AIAA.

§Professor, Control and Simulation Division, Faculty of Aerospace Engineering, P.O. Box 5058; m.mulder@tudelft.nl. Senior Member AIAA.

I. Introduction

PILOT manual-control behavior can be modeled successfully using quasi-linear models that consist of linear response functions and a remnant signal to account for nonlinearities [1–5]. The modeling and identification of pilot dynamics requires measurements that are typically taken from control tasks in which manual-control action is induced using target and disturbance forcing function signals [2,6,7]. These target and disturbance signals represent the reference trajectory that needs to be followed and external disturbances that are to be attenuated, respectively. The characteristics of these forcing function signals heavily influence the actual control behavior that is adopted and the quality of pilot model identification results. For instance, McRuer et al. [1] indicate that

random-appearing forcing function signals are required for inducing skill-based manual control. In addition, commonly used multimodal pilot model identification techniques make use of multiple independent quasi-random multisine forcing functions to be able to separate the responses to multiple cues [6].

Quasi-random target and disturbance forcing function signals have frequently been combined in tracking tasks to allow for separate modeling of pilot visual and vestibular responses [6,8,9]. Even though accurate estimates of multimodal pilot model parameters can be obtained with these identification techniques if multiple quasi-random forcing function signals are applied, this approach results in control tasks that can be considered as less representative for real-life piloting tasks. Perturbing the controlled element using a (low-pass) quasi-random disturbance signal is not objectionable due to its similarity to turbulence. The following of a quasi-random multisine target signal, however, is often indicated to be unlike any control task performed in flight.

As indicated in [10], time-domain estimation techniques for identification of multimodal pilot models put less severe constraints on the design of forcing functions. Rather than requiring an independent forcing function signal for each model channel, as needed for application of the method described in [6], data sets used for time-domain model identification only need to be "persistently exciting" [11]. This reduced requirement on forcing function design theoretically allows for alternative types of forcing functions to be used to excite a pilot–vehicle system for multimodal pilot model identification. For example, an aircraft pitch or roll attitude control task, where a multisine disturbance signal is combined with a target signal consisting of multiple discrete ramps and steps in target attitude, may also yield identifiable measurements of pilot behavior. Such target signals also yield more realistic manual-control tasks, similar to in-flight maneuvers such as turn entry or altitude change, while flying in turbulence [12,13].

Two distinct challenges, however, arise when control behavior is analyzed using such deterministic reference signals. First, the quasi-random nature of the target signal is lost, and the deterministic nature of multiramp signals may yield precognitive (feedforward) or pursuit-tracking control behavior [2,14–17]. As, for instance, argued in [2,14], control behavior in a pursuit-tracking situation is found to be a combination of pursuit (feedforward) and compensatory (error reducing) control operations. Therefore, depending on further details of control task design, predictable forcing function signals could yield a deviation from purely compensatory control, to which the multimodal pilot models that have been used to analyze control behavior [12,13,18] need to be adapted.

A second distinct challenge lies in the fact that it is unknown if such alternative forcing function signals provide enough excitation of the combined pilot–vehicle system (that is, yield data sets that are sufficiently informative) to allow for reliable separation of pilots' visual and vestibular responses [10]. This paper investigates this latter issue by evaluating the accuracy of model identification results for control tasks where a reference signal consisting of multiple ramplike changes in target attitude is followed. Unlike the experimental approach to evaluating such alternative forcing functions taken in [12,13,18], this paper will make use of pilot model simulations, based on experimental measurements taken from [12], to assess the accuracy and reliability of pilot model identification results. For this analysis, a model of purely compensatory multimodal pilot control is used, yielding a typical multimodal pilot model identification problem as, for instance, are also analyzed in [8,10]. Feedforward control strategies resulting from the use of deterministic input signals are not considered in the adopted pilot model for two reasons. First, experimental measurements supporting the presence of such control behavior are sparse, and appropriate models for describing this feedforward have not yet been validated. Moreover, the presence of feedforward control operations is largely independent of the problem of separating pilot compensatory visual and vestibular responses, as studied here. As will be shown in this paper, increased excitation of the pilot–vehicle system is obtained for increased steepness of the ramps in such alternative forcing function signals. Therefore, the effects of ramp signal steepness on the multimodal pilot model identification problem are evaluated by comparing estimation results for signals with different levels of ramp steepness.

This paper first gives an overview of the multimodal pilot model identification problem, including a description of the pilot model and identification algorithm used for estimating the model parameters. Then, Sec. III provides an analysis of the excitation provided by signals consisting of a number of ramps using frequency-domain methods. Details of the pilot model simulations, the different forcing function settings that are evaluated, and the settings of the identification algorithm are given in Sec. IV. Section V presents the main results of the identification performed on the data from the pilot model simulations. The paper ends with a discussion and conclusions.

II. Pilot Model Identification Problem

A. Control Task

During manual-control tasks in a multimodal environment, human operators may use information perceived through different perceptual modalities for feedback [3]. In addition, they may use this information to achieve compensatory control, pursuit control, precognitive control, or any combination of these modes of control operation [2]. In this paper, pilot control behavior during compensatory attitude control (tracking) tasks is investigated, based on the control task performed in the experiment described in [12]. Figure 1 shows a schematic representation of a pilot–vehicle system where a pilot performs compensatory control. Physical motion feedback, which has been shown to make a significant contribution to pilot control in multimodal environments in a number of previous investigations [6,7,19,20], is included as a second feedback channel $H_{p_m}(s)$.

Target and disturbance forcing function signals are indicated in Fig. 1 with the symbols f_t and f_d, respectively. These signals represent the reference trajectory that is to be followed and the external disturbances (turbulence) that are to be attenuated by the pilot. Pilot control action is shown to be the sum of the pilot's compensatory (visual) and motion responses, $H_{p_v}(s)$ and $H_{p_m}(s)$. The inputs to the visual and motion channels of the pilot model are the tracking error e and the state of the controlled element x, respectively. An additional remnant signal n is added to the responses of the linear pilot model channels to model the nonlinear (uncorrelated) portion of the pilot control signal, u.

In the schematic representation shown in Fig. 1, the dynamics of the controlled element are represented by $H_c(s)$. In the experi-

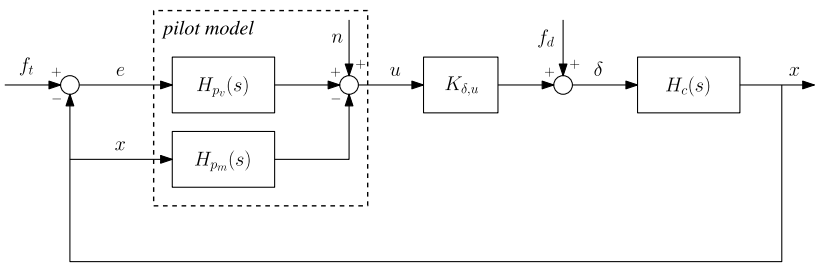

Fig. 1 Schematic representation of a multimodal attitude control task with visual and vestibular motion feedback.

ment of [12], acceleration control was considered. Therefore, the transfer function of the controlled element used in this paper is given by

$$H_c(s) = \frac{K_c}{s^2} \tag{1}$$

In Fig. 1, the symbol $K_{\delta,u}$ represents the scaling gain between the pilot control deflection u and the input to the controlled element δ. The numerical values that were used for the controlled element gain K_c and the control scaling gain $K_{\delta,u}$ in the experiment of [12], which are also applied in the current evaluation, will be specified in Sec. IV.

B. Pilot Model

Human manual-control behavior is inherently time varying and nonlinear. For carefully designed control tasks (and especially for compensatory control tasks, as the one studied in this paper), pilot control behavior can be successfully captured using quasi-linear pilot models [1,2]. During compensatory manual-control tasks, pilots are known to adapt their control strategy to the dynamics of the controlled element to achieve approximately single-integrator open-loop dynamics over a wide frequency range around gain crossover [1]. For the double-integrator dynamics defined by Eq. (1), this implies that pilots will need to generate lead starting at frequencies below crossover to compensate for the second-order dynamics of $H_c(s)$. In addition, the presence of physical motion cues has been shown to affect pilot control behavior and task performance in numerous occasions [3,5–7,19], especially for controlled elements that require pilots to perform significant lead equalization [20].

An appropriate quasi-linear multimodal pilot model that captures both compensatory visual control strategies and the effect of physical motion feedback on pilot control, as depicted in Fig. 1, is shown in Fig. 2. Note that the pilot visual and motion responses are modeled as separate parallel channels, which have the tracking error e and the system attitude x as inputs. Furthermore, note that the linear responses of both channels consist of contributions from the human motion sensory dynamics, pilot equalization dynamics, and pilot limitations (such as perceptual delays and the dynamics of the neuromuscular system). Similar pilot models have been applied in many earlier studies into human manual-control behavior in vehicle control tasks [3–5,9].

As shown in Fig. 2, it is assumed that the semicircular canals, which are part of the human vestibular organ in the inner ear, are the dominant motion sensor for perception of physical angular motion. The semicircular canals are sensitive to angular accelerations, and their dynamics can be described by [3]:

$$H_{\mathrm{scc}}(s) = K_{\mathrm{scc}} \frac{1 + 0.11s}{(1 + 5.9s)(1 + 0.005s)} \tag{2}$$

The time constants of the semicircular canal dynamics given by Eq. (2) are assumed to be constants. The main free parameters of the pilot model shown in Fig. 2 are the visual and motion perception gains, K_{p_v} and K_{p_m}, the corresponding perceptual time delays, τ_v and τ_m, and the visual lead constant T_L. The neuromuscular actuation dynamics, depicted as $H_{\mathrm{nm}}(s)$ in Fig. 2, are modeled as a second-order mass-spring-damper system:

$$H_{\mathrm{nm}}(s) = \frac{\omega_{\mathrm{nm}}^2}{s^2 + 2\zeta_{\mathrm{nm}}\omega_{\mathrm{nm}}s + \omega_{\mathrm{nm}}^2} \tag{3}$$

Previous experiments have shown that the characteristic frequency ω_{nm} and damping factor ζ_{nm} of the neuromuscular system tend to vary considerably for different control tasks [9] and motion cueing settings [5]. Therefore, both are also considered as free pilot model parameters, which gives a total of seven pilot model parameters that are to be estimated when fitting the model of Fig. 2 to measured data.

C. Parameter Estimation Procedure

This paper focuses on the reliability with which the parameters of multimodal pilot models can be identified. The main problem that is encountered when the parameters of models like the one depicted in Fig. 2 are estimated from measurement data is that these models are overdetermined [10]. This overdetermined model structure results from the fact that the semicircular canals are hypothesized to integrate perceived angular accelerations in the frequency range of interest to manual control [3], thereby yielding an additional source of pilot lead. Previous experiments have shown that pilots adopt a control strategy in which the available motion cues are used to reduce the amount of lead that is generated visually but that pilot visual lead equalization does not fully disappear [5,9]. As pointed out in [10], this may cause parameter estimation algorithms to return sets of model parameters that, for instance, attribute all pilot lead to either the visual or the vestibular pilot model channels, sometimes without significantly degrading the goodness of fit. To be able to draw valid conclusions on pilots' use of physical motion information during manual control, however, it is essential that the visual and vestibular contributions to the measured pilot control behavior can be separated reliably.

As described in detail in [8,10], different identification methods are available for estimating the parameters of multimodal pilot models from measurement data. Frequency-domain methods, such as those based on Fourier coefficients [6] and linear time-invariant models [8], first estimate nonparametric describing functions of the observed pilot control behavior. Then, in a second step, the parameters of the pilot model are identified by fitting the model to this frequency-domain data. Alternatively, time-domain parameter estimation methods, such as the maximum likelihood estimation (MLE) procedure described in [10], estimate pilot model parameters directly from time-domain measurements.

The success of the frequency-domain estimation methods is highly dependent on the design of the experiment forcing functions [8,10], f_t and f_d in Fig. 1. In fact, they require independent target and disturbance signals for successful estimation of the visual- and motion-describing functions in the first step [6], which is usually achieved by using two multisine forcing function signals with interleaving frequencies.

For time-domain estimation methods, there is no requirement for independent forcing functions, but the different inputs to the pilot model (e and x in Fig. 2) should be persistently exciting [10,11]. This implies that, for control tasks in which a disturbance signal f_d is to be attenuated, an additional target forcing function is still needed to provide enough excitation (that is, to induce differences in e and x) to allow for reliable multimodal pilot model identification. However,

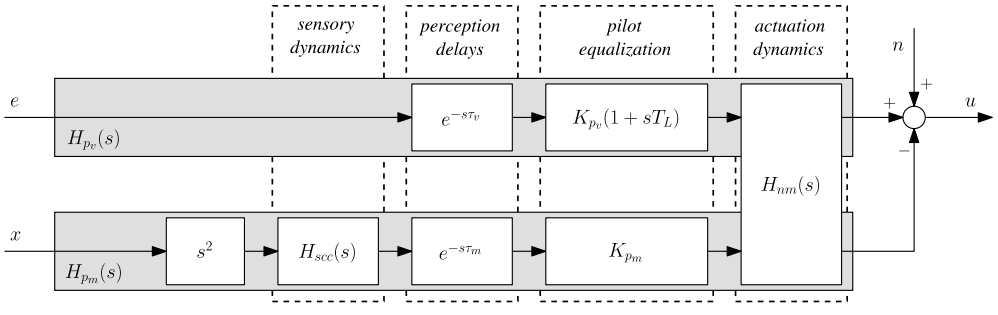

Fig. 2 Quasi-linear multimodal pilot model for compensatory attitude control.

unlike for the frequency-domain estimation methods, the target signal is not required to be an independent multisine signal. Therefore, multimodal pilot model identification with MLE [10] theoretically allows for the use of target forcing function signals consisting of multiple ramplike changes in target attitude instead of a quasi-random target signal [10,12]. It is, however, as of yet unknown if such alternative forcing function signals provide enough excitation of the pilot–vehicle system to allow for reliable estimation for the overdetermined multimodal pilot model [10,13] and how ramp signal design affects the accuracy of model identification results.

III. Ramp Forcing Function Characteristics

Ramplike and steplike input signals are successfully applied for the identification of unknown system dynamics in engineering disciplines other than multimodal pilot model identification [21–23]. As, for instance, pointed out in [24–26], the type of excitation used for gathering the data on which system identification is to be performed significantly influences the accuracy and reliability with which model parameters can be estimated. In many previous investigations into multimodal pilot control behavior, quasi-random target forcing function signals have been found to yield sufficient excitation to provide accurate pilot model identification results [5,8,9,12]. This section uses such a quasi-random multisine target signal taken from previous research [12] as a baseline for comparing the excitation provided by signals consisting of ramplike or steplike changes in target attitude. In addition, the effects of one of the design parameters that is thought to affect the excitation provided by such alternative forcing functions signals (that is, the steepness of the ramps) are evaluated in both the time and frequency domains.

A. Fourier Transforms of Ramps and Steps

Figure 3 depicts time traces of the basic building blocks of the ramp and step forcing function signals that are evaluated in this paper. Figure 3 shows signals consisting of a single step $s(t)$ and of a single ramp $r(t)$, which end at the same final magnitude as the step. Note that the magnitudes of both the ramp and the step are equal to A and that the ramp takes time T to reach that final value.

Because of the fact that the pilot model defined in Fig. 2 describes pilot dynamics over a relatively wide frequency range (0.1–20 rad/s), sufficient excitation over this frequency range is required for reliable identification of the model. To evaluate the power distributions (spectra) of the step and ramp signals shown in Fig. 3, the Fourier transform can be applied to $s(t)$ and $r(t)$, as is done in Eqs. (4) and (5), respectively:

$$s(t) = \begin{cases} 0 & t < 0 \\ A & t \geq 0 \end{cases} \Longleftrightarrow S(s) = \frac{A}{s} \tag{4}$$

$$r(t) = \begin{cases} 0 & t < 0 \\ \frac{A}{T}t & 0 \leq t < T \\ A & t \geq T \end{cases} \Longleftrightarrow R(s) = \frac{A/T}{s^2}(1 - e^{-sT}) \tag{5}$$

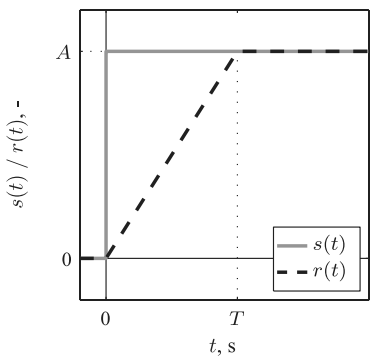

Fig. 3 Example time traces of single ramp and step signals.

Equation (4) indicates that the Fourier transform of the step signal $s(t)$ is an integrator with a gain equal to A. Similarly, the Fourier transform of the ramp signal $r(t)$ is approximately equal to a double integrator with a gain of A/T. Note that this Fourier analysis of $s(t)$ and $r(t)$ already reveals that step signals provide significantly more high-frequency excitation than ramp signals, for which the amplitude distribution decays with frequency at a rate of 40 dB per decade, compared with 20 dB per decade for $S(s)$. Equations (4) and (5) further show that the power in both $s(t)$ and $r(t)$ increases when A is increased: that is, when the magnitude of the changes in the commanded signal is larger. In addition, it can be verified from Eq. (5) that the magnitude of $R(s)$ is inversely proportional to T, which implies more signal power for steeper ramps.

The Fourier analysis of ramp and step signals presented here indicates that the amount of excitation provided by such signals can be manipulated with the parameters that define the magnitude of ramps or steps and the steepness of the ramps. In the remainder of this paper, the effect of the final parameter, ramp steepness, will be evaluated further. Signals with steplike changes, such as $s(t)$, will be treated as ramp signals with ramps of infinite steepness.

B. Comparison with Multisine Signal

This section evaluates how the excitation provided by multiramp signals (that is, the total amount of power such signals hold and how this power is distributed over the frequency content of the signal) compares to that of the quasi-random multisine signals that are often applied for multimodal pilot model identification. Multisine forcing functions are typically constructed according to

$$f_{d,t}(t) = \sum_{k=1}^{N_{d,t}} A_{d,t}(k) \sin[\omega_{d,t}(k)t + \phi_{d,t}(k)] \tag{6}$$

The subscripts d and t in Eq. (6) refer to the disturbance and target forcing functions f_d and f_t, respectively (see Fig. 1). Equation (6) indicates that these quasi-random multisine forcing functions are constructed as the sum of a number ($N_{d,t}$) of individual sinusoids. The amplitudes, frequencies, and phases of each sinusoid are indicated with the symbols $A_{d,t}(k)$, $\omega_{d,t}(k)$, and $\phi_{d,t}(k)$, respectively. The multisine forcing functions that are used in this paper are those from a previous experiment [12]. The detailed characteristics of these signals [that is, the amplitude, frequency, and phase distributions defined in Eq. (6)] will be defined in Sec. IV.B. Here, the time trace and the corresponding Fourier transform of the multisine target signal from [12] will be used for comparison with the proposed multiramp signals.

1. Time Domain

Figure 4 depicts the multisine target forcing function, from the experiment described in [12], in gray. It also shows three examples of the ramp forcing functions that are investigated in this paper.

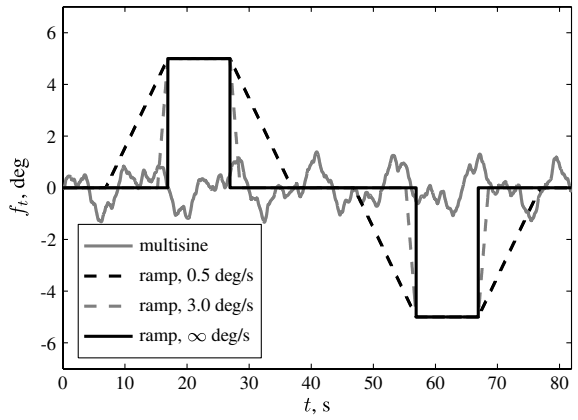

Fig. 4 Time traces of multisine and multiramp target forcing function signals.

Note that these ramp signals, all consisting of one positive and one negative excursion in commanded target value, are highly similar to those evaluated in previous investigations [12,13,18]. Furthermore, note that the amplitude of the excursions (A in Fig. 3) is chosen to be equal to 5 deg for all ramp signals. Figure 4 also shows the effect of ramp signal steepness; here, signals with steepness values of 0.5 and 3.0 deg/s, in addition to an infinitely steep ramp (step), are depicted.

2. *Frequency Domain*

From the comparison of the signal time traces in Fig. 4, the multisine target signal appears to provide a distinctly different and significantly more high-frequency excitation than the ramp signals. This is further evaluated by comparing the frequency content of the forcing function signals of Fig. 4 in the frequency domain. Figure 5 shows the absolute value of the Fourier transform of the multisine target signal. For reference, the magnitude distribution of unity-gain single and double integrators are shown alongside.

Note from Fig. 5 that the multisine target signal only provides excitation at the frequencies of the sinusoids that make up the signal (indicated with the circular markers). At all other frequencies, the multisine signal provides no power. The multisine signal amplitudes follow a low-pass distribution, as the amplitude of the sinusoid with the lowest frequency is around 0 dB, where this is reduced to around −40 dB for the highest frequency sinusoid. Such a distribution of sinusoid amplitudes, with reduced power at higher frequencies, was proposed by McRuer et al. [1] to yield signals that were not too difficult to track but still allowed for measurement of high-frequency pilot dynamics. Forcing function signals with the same amplitude distribution as depicted in Fig. 5 have been used successfully in many later investigations [5,9,18].

Figure 6 shows the absolute values of the Fourier transforms of the three ramp signals depicted in Fig. 4. Note that the single and double integrators shown in Fig. 5 are also depicted here but that, unlike Fig. 5, the vertical axes of these graphs only span [−150, 50] dB.

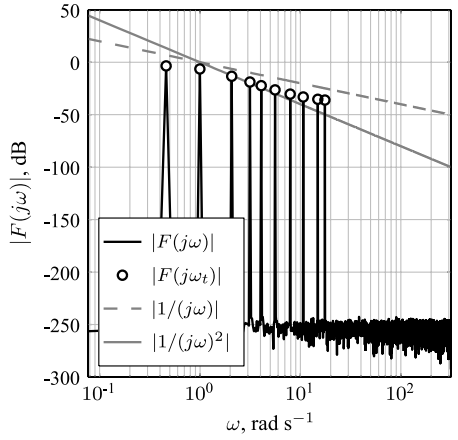

Fig. 5 Absolute value of Fourier transform of the multisine forcing function used in [12].

Comparison of Figs. 6a and 6b with Fig. 6c shows that the Fourier transforms of the signal time traces depicted in Fig. 3 abide by Eqs. (4) and (5), respectively. For both ramp signals, the absolute value of the Fourier transform is found to be approximately proportional to $|1/(j\omega)^2|$, where increased ramp signal steepness clearly yields increased signal power, as predicted by Eq. (5). Figure 6c shows that, for infinitely steep ramps, the signal amplitudes vary approximately proportional with $|1/j\omega|$, yielding comparatively more high-frequency power than Figs. 6a and 6b show for the ramp signals with lower steepness. Figure 6 thus shows that the steepness of the ramps in the alternative forcing function signals evaluated in this paper affects the (high-frequency) excitation provided by such signals.

Direct comparison of the excitation provided by multisine and multiramp signals is difficult. This is due to the fact that the signal power is distributed over a limited number of discrete frequencies for signals consisting of a number of sinusoids while, for multiramp signals, power is distributed more evenly over all frequencies (compare Figs. 5 and 6). To still allow for some comparison, the absolute values of the Fourier transforms of the different forcing function signals depicted in Figs. 5 and 6 have been averaged over a number of neighboring frequencies around the multisine signal sinusoid frequencies. As can be observed from Fig. 7, this yields 10 frequency bins (light-gray shaded areas) over which the signal power is averaged. Note that these 10 bins together contain all frequencies of the signals' Fourier transforms up to a frequency of 20 rad/s. For the multisine signal, the resulting averaged power distribution $|\bar{F}(j\omega)|$ (the gray line in Fig. 7) still follows the signal's low-pass characteristic.

The same frequency-domain averaging was also performed on the ramp signal Fourier transforms depicted in Fig. 6. Figure 8 shows a comparison of the averaged signal power $|\bar{F}(j\omega)|$ for the different forcing function signals. The average power of the multisine target forcing function signal is depicted a solid gray line, as is also done in Fig. 7. Note again from Fig. 8 that increased ramp signal steepness results in increased signal power over the full frequency range. In addition, the comparison with $|\bar{F}(j\omega)|$ for the multisine signal shown in Fig. 8 indicates that the ramp signal with a steepness of 3.0 deg/s already provides slightly more averaged power. This shows that, depending on the selection of ramp signal parameters, such ramp signals can provide excitation similar to that achieved with a multisine signal over the complete frequency range of interest, or even better.

IV. Method

To evaluate the identifiability of multimodal pilot models when using alternative target forcing functions, as depicted in Fig. 3, simulations of multimodal pilot control in a control task similar to the one described by Zaal et al. [12] are used. This approach, where the exact pilot dynamics are known, allows for quantification and

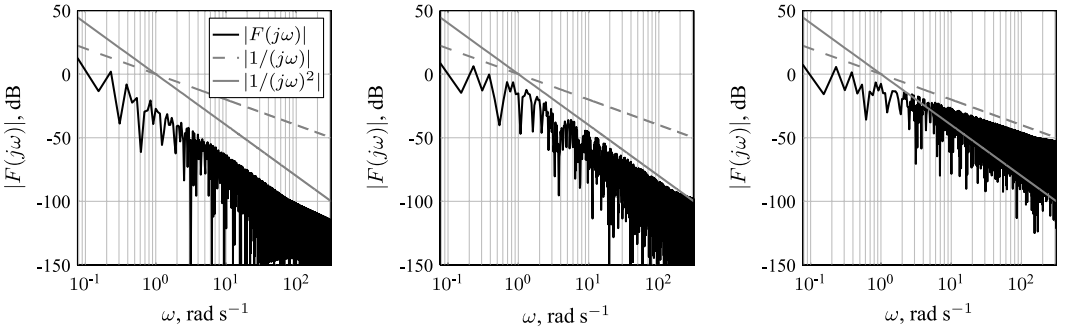

a) Ramp steepness 0.5 deg/s **b) Ramp steepness 3.0 deg/s** **c) Ramp steepness ∞ deg/s**

Fig. 6 Comparison of the absolute value of the Fourier transform for three values of ramp forcing function signal steepness.

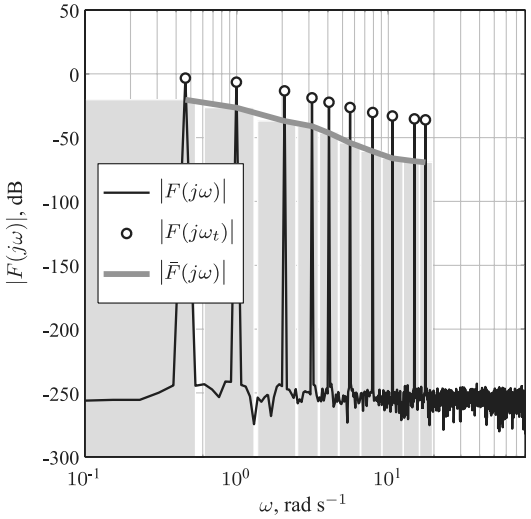

Fig. 7 Example of averaged frequency-domain power calculation using frequency bins for the multisine forcing function.

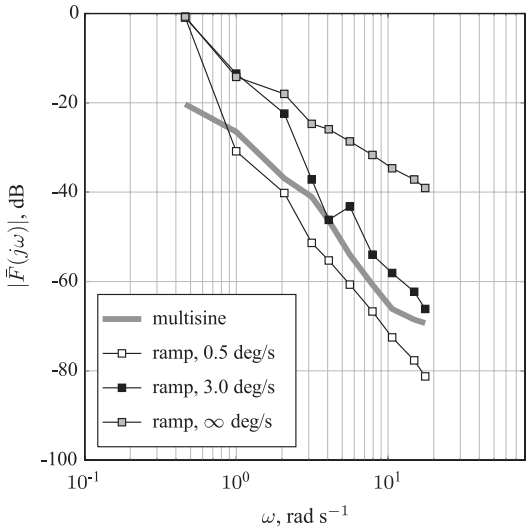

Fig. 8 Comparison of averaged frequency-domain power for multisine and ramp signals with 0.5, 3.0, and ∞ deg /s steepness.

comparison of estimation bias and variance for different forcing function settings and ramp signal steepnesses.

A. Pilot Model Simulations

To gather the data for testing the accuracy of multimodal pilot model identification results, simulations of the closed-loop control task depicted in Fig. 1 were performed. The gain of the acceleration control dynamics [Eq. (1)] was set to $K_c = 4$, and the stick input gain $K_{\delta,u}$ was chosen to be equal to 0.2865. The pilot visual and motion responses were simulated using the multimodal pilot model depicted in Fig. 2. Identified values from the experiment of Zaal et al. [12] were used for the pilot model parameters. These parameter values are listed in the top data row of Table 1.

Pilot remnant n, which is typically modeled as filtered white noise [10], was generated by passing white noise through a fourth-order low-pass filter:

$$H_n(s) = \frac{K_n}{(1 + sT_n)^4} \tag{7}$$

The chosen remnant filter gain K_n and lag time constant T_n (see Table 1) were again based on data from [12]. The remnant gain was chosen to yield a remnant contribution of 20% to the total pilot control input signal variance: that is, $\sigma_n^2/\sigma_u^2 = 0.2$ [10]. By using different white noise sequences, 100 different realizations of the multimodal control task were simulated.

B. Forcing Functions

Multisine target and disturbance forcing function signals were generated according to Eq. (6). Both f_t and f_d consisted of 10 sinusoids, for which the properties (frequencies, amplitudes, and phases) are listed in Table 2. Note that these forcing function signals are the same as those described in [12].

The disturbance signal was scaled to yield a low-pass disturbance of the controlled element output x with a variance of 1.5 deg^2. Similarly, the target signal was scaled to have a variance of 0.375 deg^2: that is, a quarter of the power of the disturbance signal. Similar fractions of target and disturbance signal power have been successfully applied in many previous experiments [5,9,12].

Five different ramp target forcing functions, like those depicted in Fig. 3, were defined, each with a different steepness of the ramps in the signals. The values for the rate of change of the ramps that were selected were 0.5, 1.0, 3.0, 10.0, and ∞ deg /s. Note that ramps with a 1.0 deg /s steepness were considered in [12,18] and that Pool et al. [13] evaluated both 1.0 and 3.0 deg /s ramp signals.

The multisine disturbance signal was present during all simulations of the control task of Fig. 1 considered here. The target forcing function was varied over seven different conditions, the five different ramp forcing functions supplemented with a multisine target signal condition and a condition with a zero target signal, for reference. The latter two conditions will be referred to in the following as MS and NO. Ramp target conditions are indicated with a capital R followed by the value of the ramp rate of change: that is, R3.0 indicates the signal with 3 deg /s ramps.

C. Identification Procedure

For the seven different control task settings described in Sec. IV.B, the known parameters of the multimodal pilot model have been

Table 2 Multisine forcing function properties

Target, f_t				Disturbance, f_d			
n_t	ω_t, rad/s	A_t, deg	ϕ_t, rad	n_d	ω_d, rad/s	A_d, deg	ϕ_d, rad
6	0.460	1.353	4.437	5	0.383	0.048	−2.088
13	0.997	0.946	2.769	11	0.844	0.175	1.238
27	2.071	0.427	1.809	23	1.764	0.381	−3.895
41	3.145	0.230	3.544	37	2.838	0.502	3.138
53	4.065	0.154	3.687	51	3.912	0.581	−2.807
73	5.599	0.096	3.209	71	5.446	0.684	−1.808
103	7.900	0.061	4.286	101	7.747	0.866	−1.563
139	10.661	0.044	2.992	137	10.508	1.152	−2.953
194	14.880	0.035	5.391	171	13.116	1.496	−2.626
229	17.564	0.032	2.006	226	17.334	2.212	0.864

Table 1 Pilot model parameters and identification of upper and lower bounds

	Pilot model							Remnant	
Parameter	K_{p_v}	T_L, s	K_{p_m}	τ_v, s	τ_m, s	ω_{nm}, rad/s	ζ_{nm}	K_n	T_n, s
Value	1.2	0.6	4.0	0.25	0.2	11.5	0.3	0.15	0.06
Identification lower bound	0.0	0.0	0.0	0.0	0.0	5.0	0.0	——	——
Identification upper bound	5.0	10.0	10.0	1.0	1.0	20.0	1.0	——	——

estimated from the simulated time traces. The time-domain MLE algorithm described in [10] was used for the identification. As also described in [10], an initial estimate of the model parameters was generated through the use of a genetic algorithm, which optimizes the model parameters for 100 iterations. The upper and lower bounds that were used for each parameter in this step of the estimation algorithm are listed in Table 1. For each realization of simulation data, this genetic optimization was performed 10 times. The best parameter estimate, as indicated by the corresponding lowest value of the likelihood function, was then further refined using an unconstrained Gauss–Newton optimization [10]. For each of the target forcing function settings, this gives a total of 100 estimated parameter sets: that is, one corresponding to each remnant realization.

D. Dependent Measures and Hypotheses

For a well-defined identification problem, repetitive maximum likelihood estimates of model parameters will have an approximately Gaussian (normal) distribution [10,27], where the mean and the standard deviation of the distribution are related to the bias and variance in the parameter estimates, respectively. Therefore, the first dependent measure that is considered here is normality of the set of 100 parameter estimates obtained for the 100 different realizations of the simulated multimodal control task. The statistical Lilliefors test [28], which compares a measured distribution to a Gaussian distribution with the same mean and standard deviation, is used to evaluate the normality of the obtained distributions of parameter estimates. In addition to testing the normality of the identified sets of parameters, the mean bias and variance of the model parameter estimates obtained for each of the seven configurations will be compared.

Because of the increased excitation provided by signals with steeper ramps (see Fig. 6), it is expected that pilot model identification results will become more consistent (that is, their distributions will become more normal) and accurate as ramp signal steepness is increased. The bias and variance in the parameter estimates are expected to be largest for the condition without target signal (NO). Based on a comparison of Figs. 5 and 6c, it is expected that the ramp signals with the highest steepnesses could yield pilot model estimates with bias and variance that are very similar to that of the estimates for the multisine target condition (MS).

V. Results

A. Example Simulation Results

Figures 9 and 10 depict example time traces of pilot model simulations for the condition with a multisine target signal and the condition with the 1.0 deg/s ramp signal (R1.0), respectively. Both Figs. 9a and 10a show the target f_t and the controlled element state x (see Fig. 1); Figs. 9b, 10b, 9c, and 10c depict the pilot control signal u (and, for reference, the remnant signal n) and the tracking error signal e. Note that the actual simulation time was 90 s (with a measurement time of 81.92 s, as defined in [12], over which the model identification was performed) but that only 60 s of the simulation data are depicted here for clarity.

Figures 9a and 10a show the difference between the target signals used for these two conditions and their effect on the controlled element state x. Note that the deviations of x from the reference trajectory defined by f_t predominantly result from the perturbations introduced by the disturbance signal f_d. As can be verified from Figs. 9b, 9c, 10b, and 10c, the pilot control and tracking error signals (u and e, respectively) are found to be highly similar for both conditions, which is again due to the same disturbance signal that is attenuated by the pilot model in both conditions. Only minor differences in both of these signals can be observed due to the different target forcing functions, mainly during the intervals where the ramp signal is increasing or decreasing.

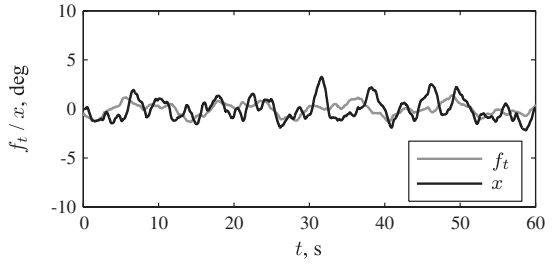

a) Target and state signal

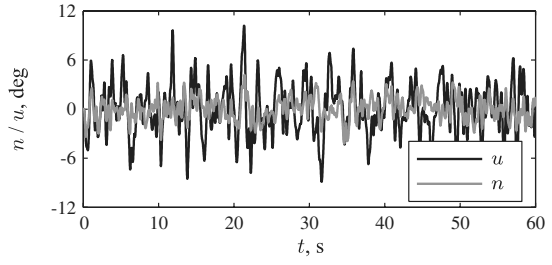

b) Control and remnant signal

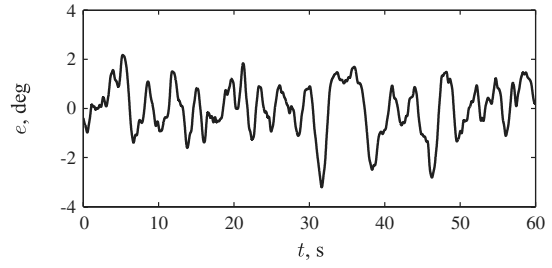

c) Error signal

Fig. 9 Example pilot model simulation time traces for condition MS.

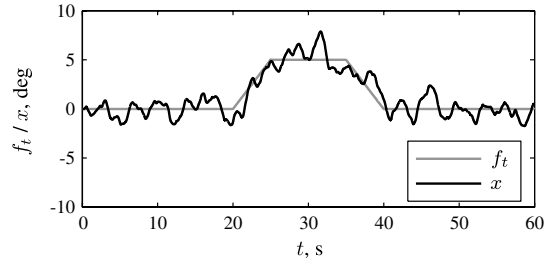

a) Target and state signal

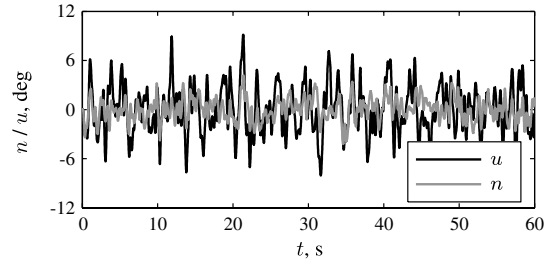

b) Control and remnant signal

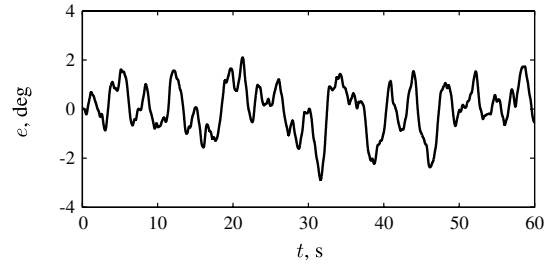

c) Error signal

Fig. 10 Example pilot model simulation time traces for condition R1.0.

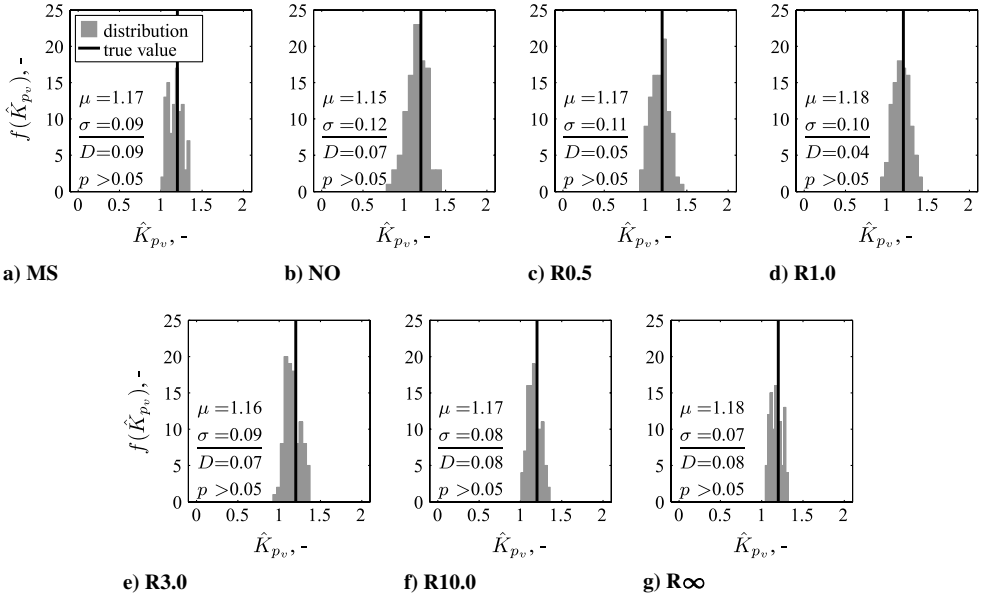

Fig. 11 Distribution of estimated values for the pilot visual gain $\hat{K}_{p_v}$ compared with its actual value, $K_{p_v} = 1.2$. Mean μ and standard deviation σ of each distribution and the Lilliefors [28] normality test statistic D and corresponding p value are listed in each graph.

B. Pilot Model Estimation Results

Using the time traces of e, x, and u, as depicted in Figs. 9 and 10, the parameters of the pilot model were estimated using MLE. This yielded a set of model parameters for each of the 100 simulations of the control task considered here. The consistency of parameter estimation results was evaluated by investigating the distribution of the different attained solutions for the different target forcing function settings. Histograms of the 100 identified values of the pilot visual gain K_{p_v}, the visual lead constant T_L, and the motion gain K_{p_m} are depicted in Figs. 11–13, respectively. The normality of the distributions shown in Figs. 11–13 has been evaluated using the Lilliefors test [28]. The values of the test statistic D and the corresponding p values are indicated in each graph. Note that a p value less than 0.05 is taken to indicate a significant deviation from normality. These figures also list the means μ and sample standard deviations σ of the presented distributions. The true values of the corresponding parameters, which were used for the pilot model simulations (see Table 1), are depicted by the solid black lines.

For the evaluation of how the distributions of the estimated parameters are affected by the variation in target forcing function signal, the results for the condition with the multisine target signal as shown in Figs. 11a, 12a, and 13a will be used as the baseline. As illustrated by these figures, the distribution of the estimated pilot model parameters that results from the use of a multisine target signal is typically not significantly different from a Gaussian distribution ($p > 0.05$), with a mean that is very close to the true parameter value. Especially for $\hat{T}_L$ and $\hat{K}_{p_m}$, when no additional target signal is used (NO), the estimated parameter values clearly show non-Gaussian distributions of parameters and a markedly larger spread (Figs. 12b and 13b). This confirms that some additional target signal is indeed needed to ensure both inputs to the multimodal pilot model are persistently exciting [11] and that the use of two independent multisine target and disturbance forcing function signals allows for obtaining reliable pilot model identification results [6,8,10].

Figures 11c–11g show the distributions of $\hat{K}_{p_v}$ for the ramp target signals with increasing ramp steepness. Based on the analysis of ramp signal characteristics in Sec. III, more consistent estimation results are expected with increasing ramp signals steepness, due to the increased excitation provided by signals with steeper ramps. As can be verified from Fig. 11, the distributions of the estimates of the pilot visual gain K_{p_v} are indeed found to become narrower (lower σ), indicative of more consistent estimates, with increasing ramp forcing function steepness. Compared with the results obtained without an additional forcing function condition (NO), as shown in Fig. 11b, the overall improvement in the estimation of K_{p_v} is, however, found to be comparatively modest. In addition, for all target forcing function settings, including the NO target condition, the distributions of $\hat{K}_{p_v}$ are found to show no significant deviations from normality ($p > 0.05$). Figure 11 therefore illustrates that the accuracy with which the pilot visual gain can be estimated from measurement data is largely independent of the applied target forcing function signal.

The distributions of the estimated values for T_L and K_{p_m}, depicted in Figs. 12 and 13, however, show a significantly more marked effect of the variation in target forcing function and ramp signal steepness. This is an expected result, as difficulties with separating the visual and vestibular contributions (pilot lead) as defined in the over-determined pilot model will first affect the identified values of these two parameters [10]. For the low-steepness ramps and, especially, the R0.5 signal, the estimates of the visual lead constant and the pilot motion gain are found to be hardly more consistent than those found without an additional target signal (NO). Note the different ranges of the vertical axes in Figs. 12b and 13b, and the additional alternative x-axis scaling of the latter. The Lilliefors test [28] results also indicate that the distributions of $\hat{T}_L$ and $\hat{K}_{p_m}$ for these conditions are non-Gaussian ($p \leq 0.05$). As ramp signal steepness is increased, however, the values of the test statistic D are seen to consistently increase, indicating reducing deviations from normality, and the distributions of the estimates of T_L and K_{p_m} become increasingly narrower. As can be verified from Figs. 12f, 12g, 13f, and 13g by evaluating the shape of the distributions and the values of D and σ, parameter estimates are even more consistent than those found with the multisine target for the two signals with the steepest ramps: that is, R10.0 and R∞.

The histograms and corresponding statistical analysis depicted in Figs. 11–13 show that the ramp signals proposed in this paper indeed provide enough power to allow for reliable estimation of the overdetermined multimodal pilot model's parameters, as long as the steepness of the ramps is above a 3.0 deg/s. Figure 14 shows the biases[¶] and standard deviations (σ in Figs. 11–13) of the estimated parameter distributions as a function of the type of target signal for all seven pilot model parameters. Note that both the bias and standard deviation are normalized with respect to the true value of the pilot model parameter and expressed as a percentage. To allow for

[¶]Note that bias is defined here as the difference between the mean of the estimated parameter values μ and the true parameter value, as both are depicted in Figs. 11–13.

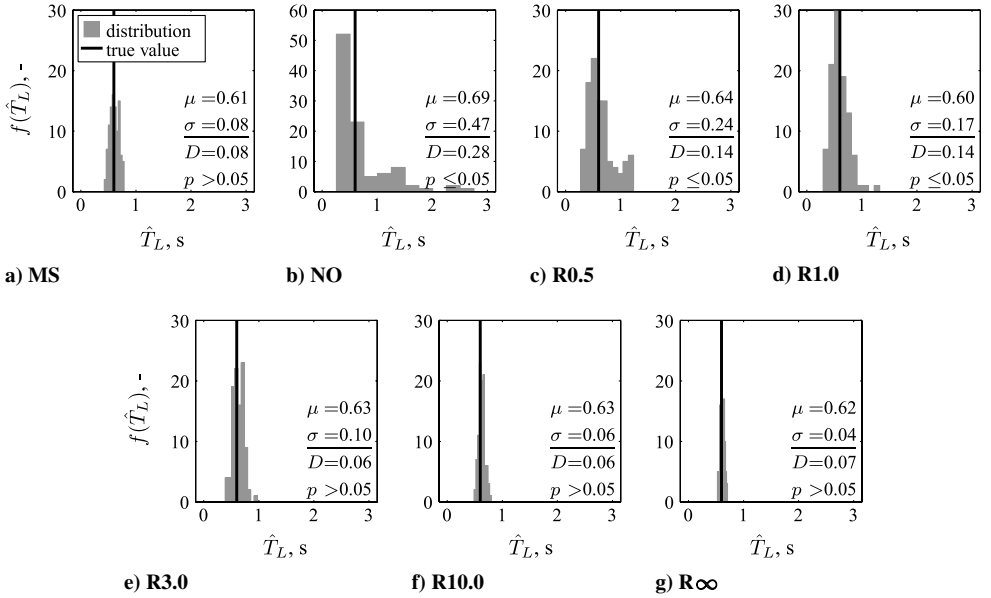

a) MS **b) NO** **c) R0.5** **d) R1.0**

e) R3.0 **f) R10.0** **g) R∞**

Fig. 12 Distribution of estimated values for the pilot lead time constant $\hat{T}_L$ compared with its actual value, $T_L = 0.6$ s. Mean μ and standard deviation σ of each distribution and the Lilliefors normality test [28] statistic D and corresponding p value are listed in each graph.

comparison with the baseline MS condition, a gray shaded area marks the bias obtained when using the multisine target signal (MS). Finally, solid black markers indicate the mean biases of those conditions for which the obtained distributions showed no significant deviations from normality, while white markers are used for those conditions for which the Lilliefors test [28] indicated a deviation from normality.

The variance bars depicted in Fig. 14 show that the spread in the estimates in all pilot model parameters reduces significantly when ramp signal steepness is increased. The fact that more narrow distributions are obtained for the steepest ramps signals than are found for the MS condition, as shown in Figs. 12 and 13, is confirmed here for the other pilot model parameters as well. For most model parameters, σ is found to be clearly lower for the R3.0 to R∞ signals than for MS. Finally, note the typically nonnormal distribution of parameter estimates and the comparatively large spread in the estimated parameter values obtained for the NO target condition and the R0.5 ramp signal; for instance, for the visual lead constant T_L and the motion delay τ_m (Figs. 14b and 14e, respectively), the variance bars cover a range of at least ±15% of the true parameter value.

In addition to this increase in estimation consistency, the bias in most parameter estimates is also seen to reduce. Note that, for the condition without an additional target signal (NO), the bias in the estimates is typically highest: on average, reaching 15–20% for the visual lead constant T_L and the visual delay τ_v (Figs. 14b and 14d, respectively) and even going up to 60% of the true parameter value for the motion delay τ_m (Fig. 14e). The decrease in bias for increased ramp steepness is perhaps most clearly visible for the estimates of both pilot model time delays, as can be verified from Figs. 14d and 14e, respectively. This can be explained by the fact that, due to the phase roll off caused by time delays, the biggest effect of these parameters is present at the higher frequencies. The increased high-frequency power in the forcing function signals for steeper ramps allows for more accurate estimation of these parameters. Note from Figs. 14d and 14e that estimates for the steepest ramps are at least as accurate as those obtained for the MS condition.

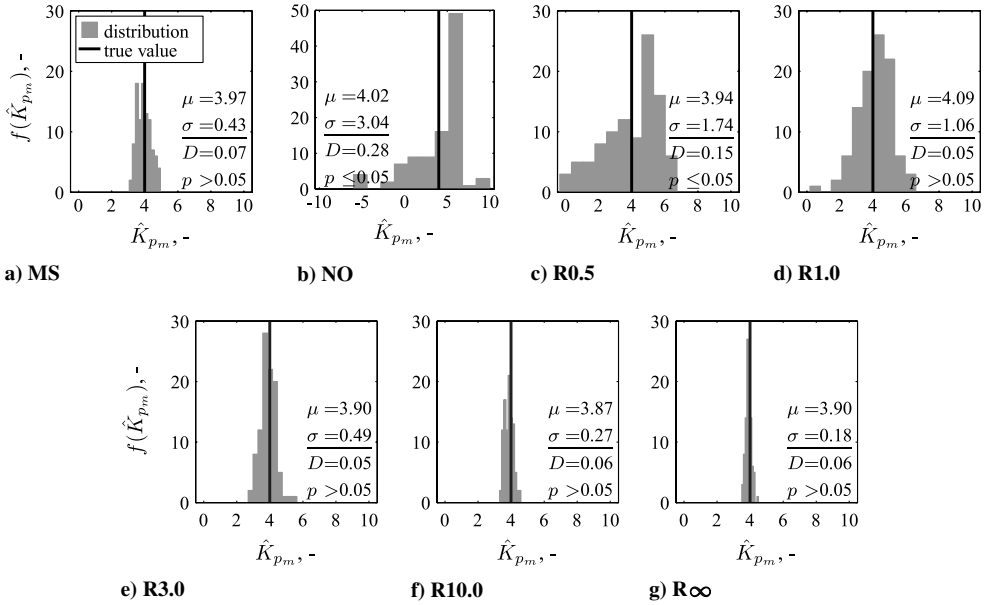

a) MS **b) NO** **c) R0.5** **d) R1.0**

e) R3.0 **f) R10.0** **g) R∞**

Fig. 13 Distribution of estimated values for the pilot motion gain $\hat{K}_{p_m}$ compared with its actual value, $K_{p_m} = 4.0$. Mean μ and standard deviation σ of each distribution and the Lilliefors normality test [28] statistic D and corresponding p value are listed in each graph.

Note that the results described here can provide an explanation for the comparatively low accuracy of the multimodal pilot model identification results found in some previous experimental evaluations in which ramp forcing function signals were evaluated [12,13,18]. In these experiments, ramp forcing function signals with steepnesses of 1.0 and 3.0 deg/s were used. Figures 11–14 suggest that the excitation provided by such signals could be insufficient to guarantee accurate and reliable pilot model identification results.

VI. Discussion

The focus of the presented research was not on the effects that target forcing function signals that consist of multiple discrete ramplike changes in reference value may have on pilot control behavior. Rather, this paper investigated whether such signals provide enough excitation to allow for reliable identification of typical overdetermined multimodal pilot models. The overdetermined models that are typically used for modeling pilot multimodal control behavior put requirements on the design of the control task and, especially, of the forcing function signals to ensure pilot modeling can be applied for analysis of pilot control behavior. In particular, sufficient high-frequency forcing function power is required for identification of the high-frequency pilot dynamics that are present in typical multimodal pilot models.

From an analysis of the proposed ramp forcing function signals in the frequency domain, using frequency-domain descriptions obtained with the Fourier transform, it was found that one of the main factors affecting the power these signals hold at higher frequencies is the steepness of the ramps in the signal. For ramp signals, the signal power is inversely proportional with the square of

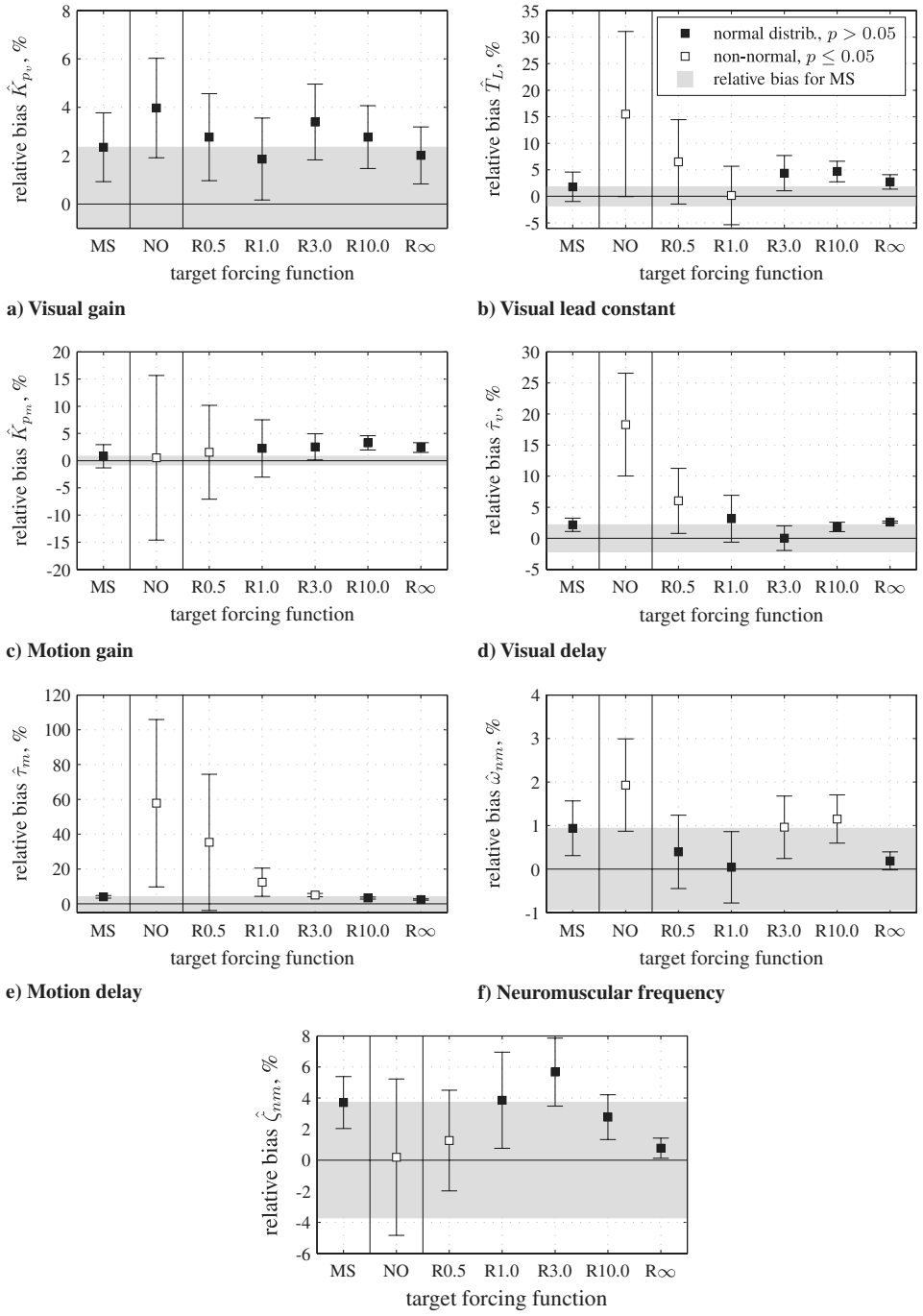

a) Visual gain **b) Visual lead constant**

c) Motion gain **d) Visual delay**

e) Motion delay **f) Neuromuscular frequency**

g) Neuromuscular damping

Fig. 14 Mean parameter estimate bias for different target forcing functions.

the frequency, but it increases approximately linearly with increased ramp signal steepness. For infinitely steep ramps, signal power is only inversely proportional to the frequency, yielding even more high-frequency excitation. Even though it is more distributed over all frequencies, on average, signals consisting of multiple ramplike changes were found to hold an amount of high-frequency power that is similar to that contained in multisine target signals that are typically used for multimodal pilot model identification.

Simulations of an attitude control task with acceleration control dynamics (double integrator) based on the results of a previous experiment [12] were used to evaluate the accuracy of multimodal pilot modeling results for different target forcing function settings. For the selected control task (defined by the choice of controlled element dynamics, pilot model parameters, and the disturbance signal f_d), a clear effect of ramp signal steepness was found on the accuracy of multimodal pilot model identification results. For ramps with steepnesses lower than 3.0 deg/s, estimated parameter values were found to have a significantly higher bias and spread than those obtained with a multisine target signal. Ramp signals with higher ramp steepnesses were, however, found to yield more reliable estimates of the multimodal pilot model parameters. This effect was visible not only in both the bias and standard deviation of the parameter estimates but also in the distribution of these estimates. Using the Lilliefors test [28], it was shown that, for conditions for which less accurate parameter estimates were obtained, distributions of parameter estimates also showed more frequent and larger deviations from normality.

The results presented in this paper indicate that the proposed ramp forcing functions can allow for reliable pilot model identification for a typical multimodal pilot model identification problem. However, it can be expected that changes in the control task (that is, variations in controlled element dynamics, forcing functions, and the adopted pilot control behavior) will affect the accuracy with which pilot model parameters can be estimated. This implies that the conclusions drawn here, with respect to the limits of ramp signal steepness, that yield accurate estimation results may differ for other control task settings. As control task and forcing function design are found to affect pilot control behavior in numerous occasions [1,3], more research is required to investigate how the results described in this paper are affected by changes in control task setup. In addition, whether the proposed ramp forcing function signals indeed provide more realistic control tasks than tracking tasks with two quasi-random forcing functions also needs to be evaluated in an experimental setting.

In this paper, the assumption was made that pilot control behavior in combined disturbance-rejection and ramp-target-signal following tasks could still be modeled using compensatory models of pilot control. As, for instance, argued in [14–16], predictable forcing function signals may yield pursuit or precognitive contributions to control behavior during tracking. It is likely that pilots will develop a mental model of the control task and the forcing function signal that will allow for feedforward control, especially if the same ramp signals are tracked a significant number of times, as was done in previous experimental investigations [12,13,18]. If ramp signal design is varied, however (for instance, by adopting randomized ramp amplitudes and durations), this would yield similar excitation to that provided by the signals considered in this paper but remove part of the predictability of the signal. This would then reduce the extent to which feedforward control is supported. These effects of using such alternative forcing function signals for modeling pilot control behavior are planned to be addressed in future experimental investigations.

VII. Conclusions

Time-domain pilot model identification techniques allow for the use of other forcing function signals than the quasi-random harmonic signals that are typically used for the identification of multimodal pilot control behavior in the frequency domain. This paper evaluated the suitability of signals consisting of multiple ramplike changes in reference value for use as the target forcing function during a manual attitude control task. The excitation and, thereby, the accuracy of multimodal pilot modeling results provided by such signals were evaluated using simulations of a typical multimodal pilot model in a control task from a previous human-in-the-loop experiment. The steepness of the ramps in such alternative forcing functions was found to heavily affect the bias and variance of the resulting pilot model parameter estimates. Steeper ramps, which were shown to contain markedly more high-frequency power, yielded significantly more reliable identification results. For the signals with the steepest ramps (>3 deg/s), estimates for most of the pilot model parameters were found to be more accurate and consistent than those obtained with a multisine target signal.

Acknowledgments

This research was supported by the Dutch Technology Foundation, the applied science division of The Netherlands Organization for Scientific Research, and the technology program of the Ministry of Economic Affairs.

References

[1] McRuer, D. T., Graham, D., Krendel, E. S., and Reisener, W., Jr., "Human Pilot Dynamics in Compensatory Systems. Theory, Models and Experiments with Controlled Element and Forcing Function Variations," Air Force Flight Dynamics Laboratory TR 65-15, Wright-Patterson AFB, OH, Aug. 1965.

[2] McRuer, D. T., and Jex, H. R., "A Review of Quasi-Linear Pilot Models," *IEEE Transactions on Human Factors in Electronics*, Vol. 8, No. 3, 1967, pp. 231–249. doi:10.1109/THFE.1967.234304

[3] Hosman, R. J. A. W., "Pilot's Perception and Control of Aircraft Motions," Ph.D. Thesis, Faculty of Aerospace Engineering, Delft University of Technology, Delft, The Netherlands, 1996.

[4] Van der Vaart, J. C., *Modelling of Perception and Action in Compensatory Manual Control Tasks*, Ph.D. Thesis, Faculty of Aerospace Engineering, Delft University of Technology, Delft, The Netherlands, 1992.

[5] Pool, D. M., Zaal, P. M. T.,Mulder, M., and Van Paassen, M. M., "Effects of Heave Washout Settings in Aircraft Pitch Disturbance Rejection," *Journal of Guidance, Control, and Dynamics*, Vol. 33, No. 1, 2010, pp. 29–41. doi:10.2514/1.46351

[6] Stapleford, R. L., Peters, R. A., and Alex, F. R., "Experiments and a Model for Pilot Dynamics with Visual and Motion Inputs," NASA CR 1325,1969.

[7] Jex, H. R., Magdaleno, R. E., and Junker, A. M., "Roll Tracking Effects of *G*-Vector Tilt and Various Types of Motion Washout," *14th Annual Conference on Manual Control*, NASA Ames Research Center, Moffett Field, CA, 1978, pp. 463–502.

[8] Nieuwenhuizen, F. M., Zaal, P. M. T., Mulder, M., Van Paassen, M. M., and Mulder, J. A., "Modeling Human Multi-Channel Motion Perception and Control Using Linear Time-Invariant Models," *Journal of Guidance, Control, and Dynamics*, Vol. 31, No. 4, 2008, pp. 999–1013. doi:10.2514/1.32307

[9] Pool, D. M., Zaal, P. M. T., Damveld, H. J., Van Paassen, M. M., and Mulder, M., "Pilot Equalization in Manual Control of Aircraft Dynamics," *Proceedings of the 2009 IEEE International Conference on Systems, Man and Cybernetics*, IEEE Publ., Piscataway, NJ, Oct. 2009, pp. 2554–2559.

[10] Zaal, P. M. T., Pool, D. M., Chu, Q. P., Van Paassen, M. M., Mulder, M., and Mulder, J. A., "Modeling Human Multimodal Perception and Control Using Genetic Maximum Likelihood Estimation," *Journal of Guidance, Control, and Dynamics*, Vol. 32, No. 4, 2009, pp. 1089–1099. doi:10.2514/1.42843

[11] Ljung, L., *System Identification Theory for the User*, 2nd ed., Prentice–Hall, Upper Saddle River, NJ, 1999.

[12] Zaal, P.M. T., Pool, D. M., Mulder,M., and Van Paassen, M. M., "New Types of Target Inputs for Multi-Modal Pilot Model Identification," AIAA Modeling and Simulation Technologies Conference and Exhibit, AIAA Paper 2008-7106, 2008.

[13] Pool, D. M., Zaal, P. M. T., Van Paassen, M. M., and Mulder, M., "Identification of Roll Attitude Control Behavior During Turn Maneuvers," Proceedings of the AIAA Modeling and Simulation Technologies Conference and Exhibit, AIAA Paper 2009-6029, 2009.

[14] Wasicko, R. J., McRuer, D. T., and Magdaleno, R. E., "Human Pilot Dynamic Response in Single-Loop Systems with Compensatory and Pursuit Displays," Air Force Flight Dynamics Laboratory TR 66-137, Wright-Patterson AFB, OH, Dec. 1966.

[15] Allen, R. W., and McRuer, D. T., "The Man/Machine Control Interface-Pursuit Control," *Automatica*, Vol. 15, No. 6, 1979, pp. 683–686. doi:10.1016/0005-1098(79)90037-2

[16] Hess, R. A., "Pursuit Tracking and Higher Levels of Skill Development in the Human Pilot," *IEEE Transactions on Systems, Man, and Cybernetics*, Vol. 11, No. 4, 1981, pp. 262–273. doi:10.1109/TSMC.1981.4308673

[17] Hess, R., "Simplified Approach for Modelling Pilot Pursuit Control Behaviour in Multi-Loop Flight Control Tasks," *Proceedings of the Institution of Mechanical Engineers, Part G, Journal of Aerospace Engineering*, Vol. 220, No. 2, 2006, pp. 85–102. doi:10.1243/09544100JAERO33

[18] Zaal, P. M. T., Pool, D. M., Mulder, M., Van Paassen, M. M., and Mulder, J. A., "Identification of Multimodal Pilot Control Behavior in Real Flight," *Journal of Guidance, Control, and Dynamics*, Vol. 33, No. 5, 2010, pp. 1527–1538. doi:10.2514/1.47908

[19] Meiry, J. L., "The Vestibular System and Human Dynamic Space Orientation," NASA CR 628, 1967.

[20] Shirley, R. S., and Young, L. R., "Motion Cues in Man-Vehicle Control," *IEEE Transactions on Man-Machine Systems*, Vol. 9, No. 4, 1968, pp. 121–128. doi:10.1109/TMMS.1968.300016

[21] Takasaki, G. M., and Fenton, R. E., "On the Identification of Vehicle Longitudinal Dynamics," *IEEE Transactions on Automatic Control*, Vol. 22, No. 4, 1977, pp. 610–615. doi:10.1109/TAC.1977.1101569

[22] Hensen, R. H. A., Van de Molengraft, M. J. G., and Steinbuch, M., "Frequency Domain Identification of Dynamic Friction Model Parameters," *IEEE Transactions on Control Systems Technology*, Vol. 10, No. 2, March 2002, pp. 191–196. doi:10.1109/87.987064

[23] Mulder, M., Lubbers, B., Zaal, P. M. T., Van Paassen, M. M., and Mulder, J. A., "Aerodynamic Hinge Moment Coefficient Estimation Using Automatic Fly-By-Wire Control Inputs," AIAA Modeling and Simulation Technologies Conference and Exhibit, AIAA Paper 2009-5692, 2009.

[24] Mehra, R. K., "Optimal Input Signals for Parameter Estimation in Dynamic Systems-Survey and New Results," *IEEE Transactions on Automatic Control*, Vol. 19, No. 6, Dec. 1974, pp. 753–768. doi:10.1109/TAC.1974.1100701

[25] Maine, R., and Iliff, K., "AGARD Flight Test Techniques Series Volume 3 on Identification of Dynamic Systems-Applications to Aircraft Part 1: The Output Error Approach," AGARD AGARDograph AG-300, North Atlantic Treaty Organization, 1986.

[26] Jategaonkar, R. V., *Flight Vehicle System Identification: A Time Domain Methodology*, Vol. 216, Progress in Astronautics and Aeronautics, AIAA, Reston, VA, Aug. 2006.

[27] Mulder, J. A., "Design and Evaluation of Dynamic Flight Test Manoeuvres," Ph.D. Thesis, Delft University of Technology, Delft, The Netherlands, 1986.

[28] Lilliefors, H. W., "On the Kolgomorov–Smirnov Test for Normality with Mean and Variance Unknown," *Journal of the American Statistical Association*, Vol. 62, No. 318, 1967, pp. 399–402. doi:10.2307/2283970